Contrib Mineral Petrol (2003) 146: 286–296
DOI 10.1007/s00410-003-0504-8

ORIGINAL PAPER

Harald Milsch · Wilhelm Heinrich · Georg Dresen

Reaction-induced fluid flow in synthetic quartz-bearing marbles

Received: 10 March 2003 / Accepted: 3 July 2003 / Published online: 24 September 2003

Abstract The reaction kinetics and fluid expulsion during the decarbonation reaction of calcite + quartz = wollastonite + CO_2 in water-absent conditions were experimentally investigated using a Paterson-type gas apparatus. Starting materials consisted of synthetic calcite/quartz rock powders with variable fractions of quartz (10, 20, and 30 wt%) and grain sizes of 10 μm (calcite) and 10 and 30 μm (quartz). Prior to reaction, samples were HIPed at 700 °C and 300 MPa confining pressure and varying pore pressures. Initial porosity was low at 2.7–6.3%, depending on pore pressure during HIP and the amount and grain size of quartz particles. Samples were annealed at reaction temperatures of 900 and 950 °C at 150 and 300 MPa confining pressures, well within the wollastonite stability field. Run durations were between 10 min and 20 h. SEM micrographs of quenched samples show growth of wollastonite rims on quartz grains and CO_2-filled pores between rims and calcite grains and along calcite grain boundaries. Measured widths of wollastonite rims vs. time indicate a parabolic growth law. The reaction is diffusion-controlled and reaction progress and CO_2 production are continuous. Porosity increases rapidly at initial stages of the reaction and attains about 10–12% after a few hours. Permeability at high reaction temperatures is below the detection limit of 10^{-21} m^2 and not affected by increased porosity. This makes persistent pore connectivity improbable, in agreement with observed fluid inclusion trails in form of unconnected pores in SEM micrographs. Release of CO_2 from the sample was measured in a downstream reservoir. The most striking observation is that fluid release is not continuous but occurs episodic and in pulses. Ongoing continuous reaction produces increase in pore pressure, which is, once having attained a critical value (P_{crit}), spontaneously released. Connectivity of the pore space is short-lived and transient. The resulting cycle includes pore pressure build-up, formation of a local crack network, pore pressure release and crack closure. Using existing models for plastic stretching and decrepitation of pores along with critical stress intensity factors for the calcite matrix and measured pore widths, it results that P_{crit} is about 20 MPa. Patterns of fluid flow based on mineralogical and stable isotope evidence are commonly predicted using the simplifying assumption of a continuous and constant porosity and permeability during decarbonation of the rock. However, simple flow models, which assume constant pore pressure, constant fluid filled porosity, and constant permeability may not commonly apply. Properties are often transient and it is most likely that fluid flow in a specific reacting rock volume is a short-lived episodic process.

Editorial responsibility: J. Hoefs

H. Milsch
Lamont-Doherty Earth Observatory,
61 Route 9 W, Palisades,
NY 10964 USA

W. Heinrich · G. Dresen (✉)
GeoForschungsZentrum Potsdam,
Telegrafenberg,
14473 Potsdam, Germany
E-mail: dre@gfz-potsdam.de
Tel.: +49-331-2881320
Fax: +49-331-2881328

Introduction

Metamorphic fluids produced by devolatilization reactions exert a strong influence on the petrological, structural and mechanical evolution of the Earth's lithosphere (Etheridge et al. 1983, 1984; Ferry 1994). The kinetics of mineral reactions are accelerated in the presence of aqueous fluids potentially reducing the ductile strength of rocks (White and Knipe 1978), and fluid expulsion from metamorphic reactions may induce variations in effective pressure leading to rock failure and seismic activity of faults (e.g. Hickman and Evans 1987; Scholz et al. 1973). In particular, dehydration reactions releasing water have been suggested to promote earthquakes in the seismogenic part of subduction

zones down to a depth of about 300 km at high lithostatic pressures (e.g. Kirby et al. 1996; Raleigh and Paterson 1965). For many devolatilization reactions the slope of the equilibrium curve is positive in pressure-temperature (P–T) space at low to moderate pressures (Fig. 1) indicating a net volume increase ΔV of the reaction products. For example, breakdown of hydrous minerals produces substantial fluid volumes, and in the case of serpentine up to 13 wt% H_2O will be released. If not allowed to escape, the generated fluid will increase the pore fluid pressure P_f prevailing in the rock and reduce the effective mean pressure: $P_{eff} = P_c - P_f$. The mechanical effect expected from devolatilization reactions is mainly through this pore pressure increase that will potentially cause rock fracturing and frictional sliding of faults.

At elevated pressures and temperatures rock deformation and devolatilization occur concurrently. Consequently, the pore pressure evolution in the rock is affected by temporal and spatial changes in porosity and permeability (Walther and Orville 1982; Wong et al. 1997). Porosity production occurs primarily through a loss in solid volume from the reaction. In addition, inelastic deformation of the rock may result in dilatant cracking and stretching of pores (Brace et al. 1966; Wanamaker and Evans 1989). In contrast, hydrostatic pressure induces elastic compaction of a porous rock and promotes brittle or plastic pore collapse (Baud et al. 2000) that may be enhanced if the rock is subjected to deviatoric stresses. However, if the pore space is completely filled the rock can only compact when the fluid is expelled. In general, compaction could be rate-limited either by deformation of the rock matrix or the fluid transport rate, which in turn is affected by transient changes in permeability.

Only a few experimental studies exist that investigate the effect of a fluid-producing metamorphic reaction on the temporal evolution of strength, pore pressure and permeability. Ko et al. (1995, 1997) and Olgaard et al. (1995) studied pore pressure evolution during dehydration of gypsum, and Rutter and Brodie (1988) investigated the dehydration of serpentinite at controlled pore pressures. These studies show a complex mechanical behavior displaying brittle fracture, cataclastic flow and plastic deformation that is intimately coupled to transient changes in transport properties of the rock. The experiments show that the strength of the rock matrix is significantly affected by variation in effective pressures and the formation of fine-grained solid reaction products. Zhang et al. (2000) measured permeability during decarbonation of quartz-bearing marbles. At very high initial porosities of 20%, they found fast reaction kinetics in the presence of water and at pressures close to lithostatic. At the lower temperatures of their experiments samples were more permeable and fluid release was continuous. Likewise, Feenstra and Wunder (2002) observed that dehydration of diasporite to form corundite embedded in marbles was fast and resulted in formation of a high-porosity zone. In natural metakarst bauxite deposits, this reaction produced similar high-porosity zones that served as efficient fluid pathways (Urai and Feenstra 2001). Excess pore pressures and microcrack formation has also been observed experimentally during partial melting of metaquartzites (Connolly et al. 1997). Permeability estimates of the crack network were roughly four orders of magnitude greater than permeabilities characteristic for typical metamorphic dehydration fluxes ranging from 10^{-19}–10^{-21} m^2 (Thompson 1997).

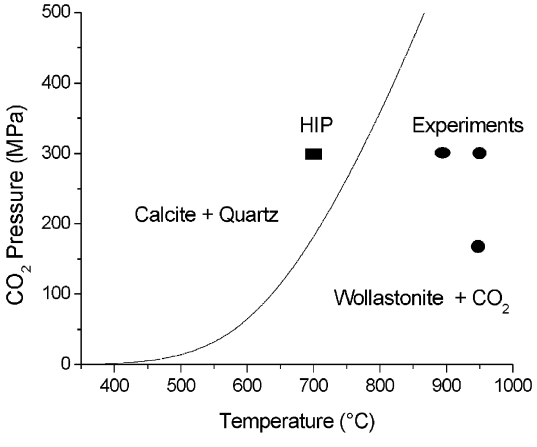

Fig. 1 Pressure-temperature equilibrium curve for the reaction calcite + quartz = wollastonite + CO_2 calculated using the internally consistent data set of Gottschalk (1997). *Square* indicates HIP conditions of the unreacted rock powder. *Circles* denote experimental annealing conditions

Interaction of reaction-induced changes of pore fluid pressure with dilational deformation could result in pulsed fluid flow through a rock matrix with initially low background permeability (Connolly 1997). The results of this model suggest that episodic flow is associated with the propagation of a porosity wave with dilation occurring at the front and compaction at the trailing edge. Plastic flow may accommodate dilation unless reaction rates become too high promoting the formation of cracks. Numerical modeling of coupled dehydration, porosity production and permeability evolution in a nominally drained system indicates development of a transient pore pressure pulse that could attain values equal to confining pressure, but will subsequently decay (Wong et al. 1997). If the fluid cannot escape and reaction rates are fast, effective pressures rapidly approach zero causing embrittlement. Whether or not pore pressure excess may be maintained for some time depends on permeability evolution. Experimental and modeling studies show that cracks grow and permeability increases rapidly with decreasing effective pressures, thus effectively eliminating fluid overpressures (Fischer and Paterson 1992; Miller and Nur 2000; Simpson et al. 2001).

In this study, we experimentally investigate fluid expulsion from a quartz-bearing synthetic marble undergoing a common metamorphic reaction:

– $Calcite + Quartz = Wollastonite + CO_2$
– $CaCO_3 + SiO_2 = CaSiO_3 + CO_2$

We studied transient changes in porosity and permeability in a dense synthetic rock with low initial porosity at high temperatures and varying effective pressures. The wollastonite-forming decarbonation reaction often occurs in contact and regional metamorphic settings (e.g. Rumble et al. 1982; Joesten and Fisher 1988; Heinrich et al. 1995) and reaction kinetics are well studied (Tanner et al. 1985; Milke and Heinrich 2002). The volume change of the solids associated with this reaction is negative (−33%), but the total volume change ΔV is positive owing to the large molar volume of CO_2 at relevant P-T conditions (Fig. 1).

Starting material and experimental procedures

Starting material

Samples were prepared from reagent grade calcite and quartz mineral powders. The arithmetic mean grain size of calcite and quartz particles was 10(±5) μm and 30(±5) μm, respectively. Some mixtures contained quartz particles with an average grain size of 10(±5) μm. The quartz content of the samples was 10, 20, and 30 wt%, respectively. Powders were stirred by hand in ethanol for 1 h to produce homogeneous mixtures and subsequently dried for more than 24 h at 120 °C. The powder was cold-pressed into thin-walled cylindrical steel sleeves of 10 mm diameter and 20 mm length.

Samples were hot-isostatically pressed (HIPed) in a Paterson-type gas medium apparatus within the stability field of calcite and quartz at a temperature of 700 °C and a confining pressure of 300 MPa for 2 h (Fig. 1). Specimens were placed between spacers with a central bore connected to a pore fluid system (Fig. 2). Pore pressure was generated by a volumometer at the upstream end of the pore fluid system using argon, and the pore pressure was measured in the upstream and downstream reservoirs of the system. During HIP, argon pore pressure was maintained at either 0.1 or 50 MPa. Consequently, effective pressures during HIP were about 300 and 250 MPa, respectively, at least as long as the pore space remained connected.

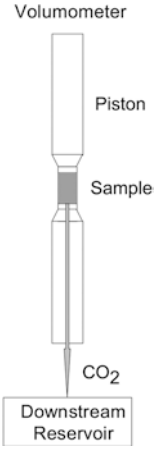

Fig. 2 Specimen assembly setup inside a Paterson-type gas medium apparatus used for HIP and annealing experiments. Samples were placed between spacers with a central bore connected to a pore fluid system. Pore pressure was generated by a volumometer and monitored upstream and downstream. During anneals pore pressure changes in the isolated downstream reservoir were used to monitor reaction-induced CO_2 expulsion from the sample chamber

Porosity of HIPed samples was measured using Archimedes' method and immersion in water and ethanol. The total unconnected porosity of HIPed samples was from 2.7 to about 6%, depending on quartz to calcite ratio and pore pressure during HIP. About ten measurements per specimen were performed and the uncertainty of total porosity values is about ±20%. This is probably due to small sample size and partial fluid penetration of the pore space during immersion.

Scanning electron microscopy (SEM) indicates that no wollastonite is present in the HIPed starting material. Samples HIPed at 50 MPa pore pressure, contain numerous small pores in the μm range located along grain and phase boundaries and also in calcite grains. Pores are less frequent in samples HIPed at 0.1 MPa pore pressure (Fig. 3a, b). Larger pores are typically confined to the quartz/calcite interface. Calcite grain boundaries are mostly straight or smoothly curved. Fragments of pure calcite aggregates show pores on grain boundaries and grain triple junctions suggesting that pores are isolated with dihedral angles >60°. Dispersion of quartz particles in the calcite matrix is relatively homogeneous. The quartz grains often contain cracks possibly owing to the highly anisotropic thermal expansion of quartz.

Experimental and analytical procedure

Samples were annealed at dry conditions at reaction temperatures of 900 and 950 °C within the stability field of wollastonite + CO_2. These conditions are far above the equilibrium curve of the reaction calculated with the internally consistent thermodynamic dataset of Gottschalk (1997) at all pressures (Fig. 1). Heat-up to annealing temperatures required about 30 min.

At each temperature a series of different anneals with durations from 1–20 h were performed to constrain reaction kinetics. During the anneals, confining pressure was maintained at 300 and 150 MPa, respectively. Initial argon pore pressure in the pore pressure system was kept at 0.1 and 50 MPa, respectively (Table 1). After annealing, samples were cooled to room temperature at pressure at 30 °C/min.

During the high-temperature anneals specimens were isolated from the upstream reservoir of the pore fluid system (Fig. 2). Downstream pore pressure changes were used to monitor reaction-induced CO_2 expulsion from the sample chamber. Pore pressure changes were measured with a resolution of 4 kPa. The reaction turnover and the total volume of the reaction products was estimated from the wollastonite rim thickness measured in SEM micrographs. We assumed zero porosity within the reaction rims and spherical wollastonite shells of constant thickness surrounding quartz particles.

To determine sample permeability, the pore pressure oscillation technique was applied (Fischer 1992; Fischer and Paterson 1992). A volumometer connected to the upstream reservoir was used to generate a sinusoidal pressure pulse of ±5 MPa superposed on an argon background pore pressure of 50 MPa. Permeability was determined from phase shift and attenuation of the pulse monitored in the downstream reservoir.

Results

The experimental conditions, measured porosities, permeabilities, and the produced amount of CO_2 calculated from wollastonite rim widths are summarized in Table 1.

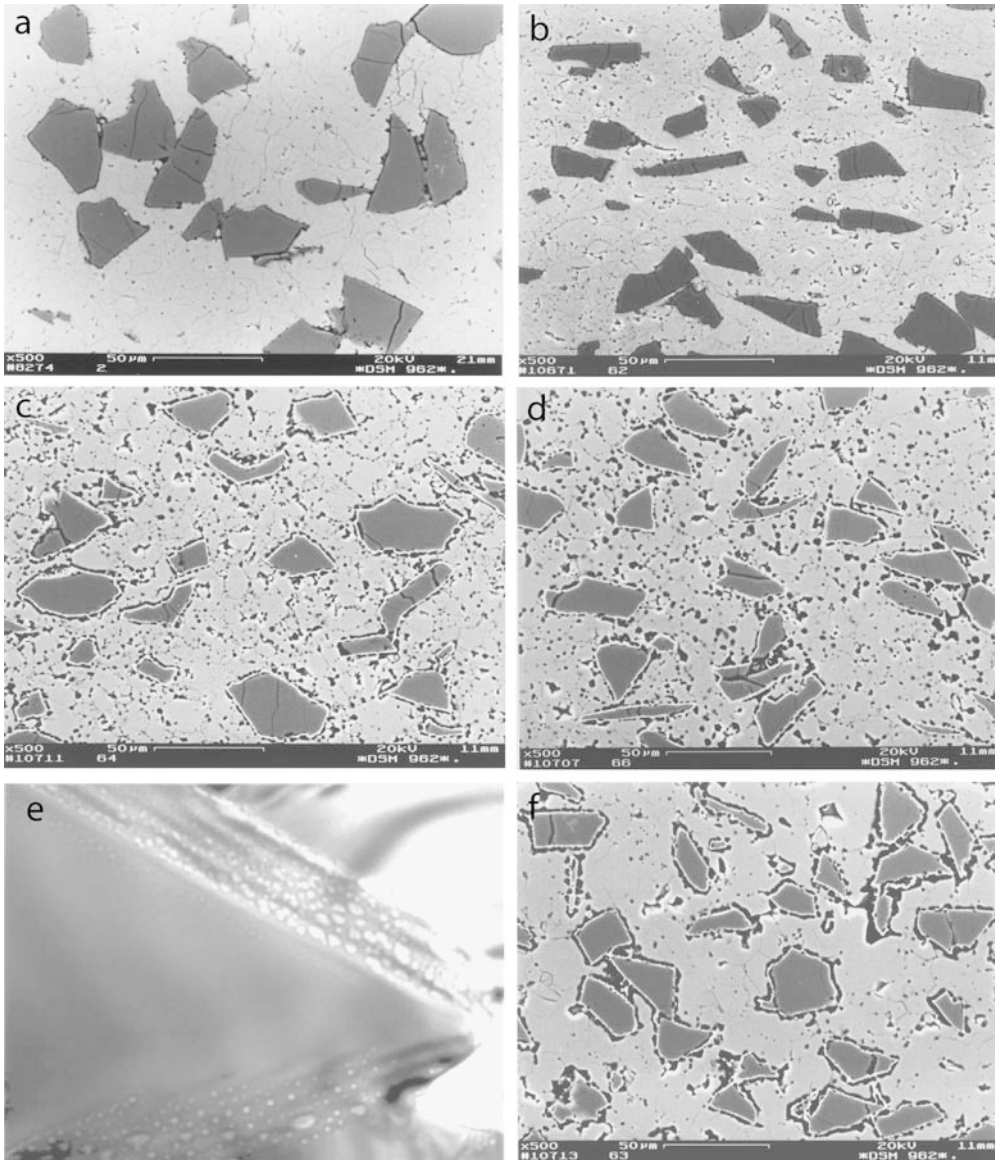

Fig. 3 Backscattered SEM and TEM micrographs of starting materials and reaction products. **a** Starting material after HIP at 0.1 MPa pore pressure for 2 h at 300 MPa confining pressure, and 700 °C (run no. 23). Angular quartz particles are *dark grey*. The quartz content is 20 wt% with average grain size of 30 μm. **b** Starting material after HIP at 50 MPa pore pressure (run no. 24). Samples contain more pores compared to **a**. **c** Aggregate HIPed at 50 MPa pore pressure and subsequently annealed at 950 °C for 5 h (20 wt% quartz particles with an average diameter of 30 μm; run no. 76). Note white rims of fibrous wollastonite grown on quartz grains indicating absence of H_2O. Numerous pores are located at phase and grain boundaries in the calcite matrix. **d** as for **c**, annealing time was 20 h (run no. 83). The size of pores and the wollastonite rim thickness increase with annealing time, i.e. with proceeding reaction. **e** TEM micrograph of a wollastonite-bearing sample (run no. 80) annealed at 950 °C for 15 h. Abundant nm-sized pores decorate grain boundaries between calcite grains. Top margin is 0.65 μm. **f** Aggregate HIPed at 300 MPa confining pressure with a pore pressure of 0.1 MPa (20 wt% quartz; run no. 79). Subsequent annealing at 950 °C was for 15 h. Note large pores located at the quartz-calcite phase boundaries and fewer pores in the calcite matrix

Microstructural evolution

Backscattered SEM micrographs of annealed samples clearly show growth of wollastonite rims on quartz grains in all experiments indicating low water content or completely dry conditions (Fig. 3c, d; see also Milke and Heinrich 2002). With increasing time during annealing, the thickness of wollastonite rims increases and pores located on calcite grain boundaries and on quartz-calcite interfaces become larger. Rim thicknesses of 2 μm are obtained within a maximum annealing time of 20 h at 950 °C. The pores form strings along grain boundaries and may result from healed cracks. This is supported by transmission electron microscope observations of grain boundaries showing abundant small pores on the micrometer to nanometer scale decorating grain boundaries (Fig. 3e). During anneals of samples HIPed with 50 MPa pore pressure, the average calcite grain size

Table 1 Experimental conditions, porosities, permeabilities, and moles of CO_2 calculated from wollastonite rim widths. All samples were HIPed at 700 °C and 300 MPa confining pressure

Run No.	Qtz amount (wt%)	Qtz size (mm)	HIP Ar pore pressure (MPa)	Mean porosity after HIP (%)	Temperature (°C)	Confining pressure (MPa)	Duration (h)	Porosity after reaction (%)	Permeability ($\times 10^{-21}$ m^2)	n(CO_2) from Wo rim width ($\times 10^{-3}$ mol)
24	20	30	50	5.2	-	-	-	-	-	-
72	20	30	50	5.2	950	300	0.16	6.5	n.d	n. d.
73	20	30	50	5.2	950	300	3	10.6	n.d	0.46
76	20	30	50	5.2	950	300	5	11.5	n.d	0.74
77	20	30	50	5.2	950	300	7	11.0	n.d	0.74
78	20	30	50	5.2	950	300	10	11.0	n.d	0.62
80	20	30	50	5.2	950	300	15	9.8	n.d	0.80
83	20	30	50	5.2	950	300	20	11.8	n.d	0.88
29	30	30	50	5.5	-	-	-	-	7.1	-
30	30	30	50	6.3	-	-	-	-	-	-
95	30	30	50	5.9	950	150	0.16	10.8	50	0.51
96	30	30	50	5.9	950	150	0.16	9.0	173	0.69
97	30	30	50	5.9	950	150	0.5	8.9	5.8	0.94
98	30	30	50	5.9	950	150	2.5	10.2	6.8	1.17
99	30	30	50	5.9	950	150	4	10.7	1.9	1.31
100	30	30	50	5.9	950	150	7	11.4	1.8	1.60
78	20	30	50	5.2	950	300	10	11.0	n.d	0.62
64	20	30	50	5.2	900	300	15	11.5	n.d	0.65
103	30	30	50	5.9	950	300	10	10.7	n.d	1.09
78	20	30	50	5.2	950	300	10	11.0	n.d	0.62
33	10	30	5	5.3	950	300	15	12.0	n.d	0.53
93	20	10	50	5.2	950	300	15	15.0	n.d	1.40
78	20	30	50	5.2	950	300	10	11.0	n.d	0.62
90	20	10	50	5.2	950	150	15	12.7	n.d	1.64
93	20	10	50	5.2	950	300	15	15.0	n.d	1.40
23	20	30	0.1	2.7	-	-	-	-	-	-
79	20	30	0.1	2.7	950	300	15	10.3	n.d	0.60

remains constant, possibly because grain boundaries are pinned by small pores. In samples HIPed at 0.1 MPa pore pressure, pores located at quartz-calcite phase boundaries are significantly larger (Fig. 3f). Initially, fewer pores were observed in the calcite matrix of these samples (Fig. 3a).

Reaction kinetics

Measured widths of wollastonite rims versus reaction duration at given temperature and confining pressure show that rim growth follows a perfect parabolic growth law. This indicates that the reaction is diffusion-controlled. Reaction progress and CO_2 production are continuous at temperatures above 800 °C for fluid pressures less than 300 MPa (Harker and Tuttle 1956; Tanner et al. 1985). Results of the reaction kinetics are documented elsewhere (Milsch 2000; Milke and Heinrich 2002).

Porosity and permeability

Porosity was measured for samples annealed at 950 °C up to 20 h. A significant increase in total porosity was observed in samples as reaction proceeded at confining pressures of 300 and 150 MPa (Fig. 4). For both pressure conditions the porosity after 0.5–4 h annealing attained values between 10 ± 2–$12 \pm 2\%$, i.e. twice the starting porosity. After a strong initial increase, porosities remained almost constant for longer reaction periods.

At temperatures ≥ 900 °C sample permeabilities were generally $< 0.3 \times 10^{-21}$ m^2. Since measurement of such low permeabilities requires measurement periods > 1 h, fast and transient changes in permeability, which may have occurred during the reaction were not resolved.

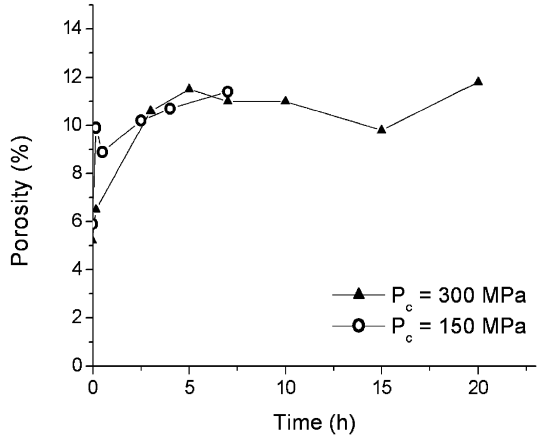

Fig. 4 Evolution of porosity with time for samples annealed at 950 °C, and confining pressures of 300, and 150 MPa, respectively (values from Table 1). Uncertainty in the porosity measurements is $\pm 20\%$

Permeability measurements performed on samples after cooling to room temperature at effective pressures of 100 MPa ranged between about $1–200\times10^{-21}$ m^2 (Table 1).

To illustrate permeability reduction during HIP of the starting material at 250 MPa effective pressure, a pore pressure pulse of ± 5 MPa was imposed during heat-up to 700 °C and densification of a calcite-quartz aggregate containing 30% quartz. After pressurizing and before heating, porosity of the sample was about 13%. The amplitude of the sinusoidal downstream pressure signal started to decay significantly at temperatures >550 °C (Fig. 5). Concomitantly, permeabilities decreased from 2.7×10^{-16} m^2 to 3.0×10^{-19} m^2 between 550C and 650 °C, respectively. At temperatures >650 °C, permeability dropped below 0.3×10^{-21} m^2, the lower resolution limit of our setup. The final porosity of the sample was 6%.

Pore pressure evolution and fluid expulsion

Since the decarbonation reaction proceeds continuously, the amount of produced CO_2 increases with time and depends on temperature, quartz content and quartz particle size. However, fluid release from the sample as monitored by a change in downstream pore pressure is not continuous but occurs stepwise (Fig. 6a–c). Pore fluid release is enhanced with increasing temperature since reaction kinetics depends strongly on temperature (Fig. 6a; Milke and Heinrich 2002). The rate of CO_2 expulsion increases with increasing quartz content of samples (Fig. 6b) and decreasing particle size (Fig. 6c), as the reactive quartz surface is increased. Commonly, pore pressure increase is small initially and then accelerates with varying step size. Fluid release is affected significantly by the sample fabrication procedure and initial microstructure of the samples. Specimens that were HIPed at 300 MPa confining pressure with 0.1 MPa pore pressure having lower porosities than those HIPed with 50 MPa pore pressure also show substantially lower pressure increase in the pore pressure system (Fig. 6d). This indicates that fluid is released more readily from samples with high initial porosity. A smaller confining pressure during annealing reduces the initial delay of the pore pressure response and significantly increases the final pore pressure, indicating a larger fluid volume released from the sample (Fig. 6e). In all experiments, the size of pore pressure steps decreases as the reaction proceeds, and the overall shape of the curves in Fig. 6a–e is sigmoidal. A decrease in the rate of fluid release with time is expected because the decarbonation reaction follows diffusion-controlled kinetics.

The measured thickness of the wollastonite rims around quartz grains was used to estimate the reaction progress and the amount of CO_2 that was produced. This fluid volume is compared to the molar amount of CO_2 released to the pore pressure system (Fig. 7a, b). It is obvious from Fig. 7 that fluid expulsion was more effective at lower confining pressures and almost complete at 150 MPa.

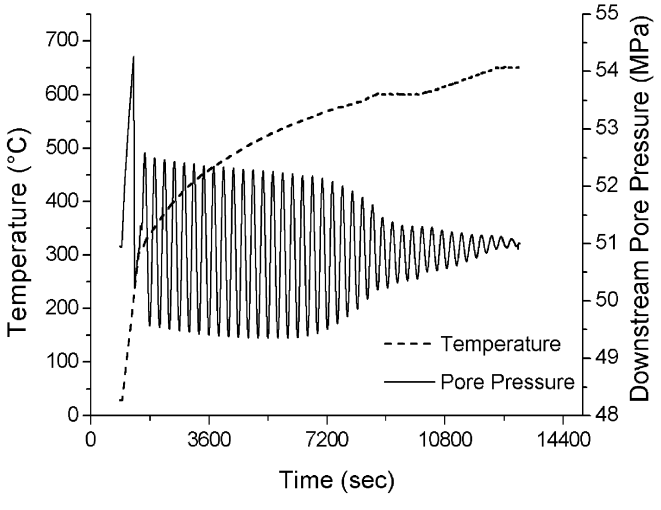

Fig. 5 Temporal decay of the downstream pore pressure signal with increasing temperature during hot isostatic pressing of a calcite/quartz aggregate, containing 30 wt% quartz

Discussion

Episodic CO_2 release and critical porosity

The striking observation from these experiments is that release of CO_2 during annealing in the stability field of wollastonite occurs predominantly episodic. The observed pore pressure steps vary significantly in size, but are always larger than the lower resolution limit of 4 kPa of the downstream pressure cell. The pore pressure evolution displays an overall sigmoidal shape (Fig. 6a–e), indicating three stages of the reaction: (1) sluggish pore pressure increase at the onset of the reaction, followed by (2) a stage of maximum fluid release, and (3) a slow-down of pore pressure increase during the later stages of the reaction. This was also observed by Ko et al. (1997) during experimental dehydration of gypsum, although in their experiments the fluid release mechanism is different. In our experiments, pressure was monitored in the downstream reservoir and the CO_2 was expelled from the sample bottom end.

Permeability of the samples at temperatures >650 °C is very low at $k<0.3\times10^{-21}$ m^2, indicating that the samples were essentially impermeable at the start of the reaction (Fig. 5). The porosity of samples annealed at 650 °C was about 5–6%. This suggests that for porosities less than about 5% pores are disconnected, in very good agreement with critical porosities given for pure calcite aggregates of 5 and 4% (Bernabé et al. 1982; Zhang et al. 1994). However, the significant increase in porosity observed after annealing (Fig. 4) does not affect

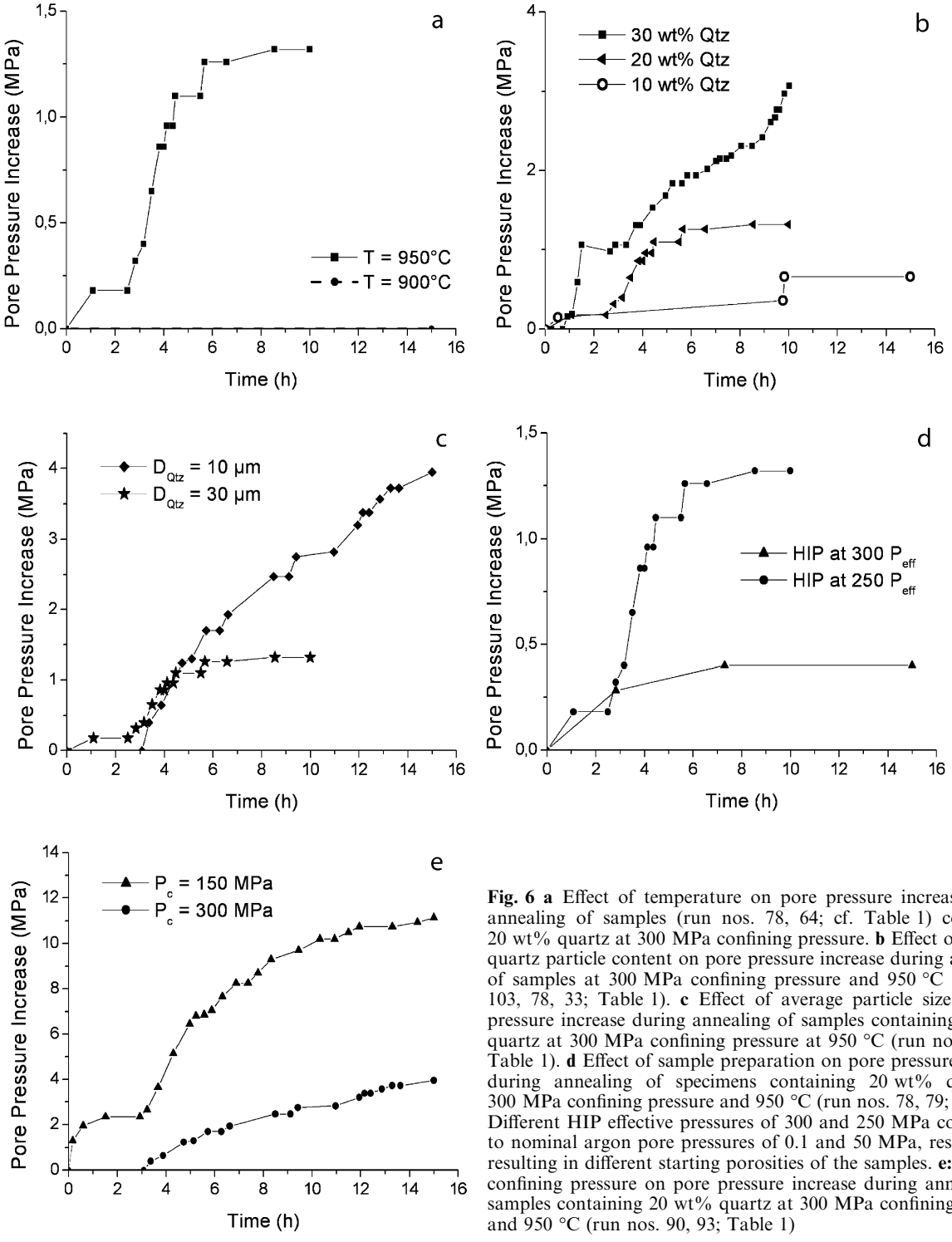

Fig. 6 **a** Effect of temperature on pore pressure increase during annealing of samples (run nos. 78, 64; cf. Table 1) containing 20 wt% quartz at 300 MPa confining pressure. **b** Effect of average quartz particle content on pore pressure increase during annealing of samples at 300 MPa confining pressure and 950 °C (run nos. 103, 78, 33; Table 1). **c** Effect of average particle size on pore pressure increase during annealing of samples containing 20 wt% quartz at 300 MPa confining pressure at 950 °C (run nos. 93, 78; Table 1). **d** Effect of sample preparation on pore pressure increase during annealing of specimens containing 20 wt% quartz at 300 MPa confining pressure and 950 °C (run nos. 78, 79; Table 1). Different HIP effective pressures of 300 and 250 MPa correspond to nominal argon pore pressures of 0.1 and 50 MPa, respectively, resulting in different starting porosities of the samples. **e:** Effect of confining pressure on pore pressure increase during annealing of samples containing 20 wt% quartz at 300 MPa confining pressure and 950 °C (run nos. 90, 93; Table 1)

sample permeability. This is in contrast to existing models predicting a percolation threshold and loss of pore connectivity at a porosity of about 4% (i.e. Zhang et al. 1994). Instead, our data suggest that pores remain disconnected even at porosities that are larger than 8% (Fig. 4). Microstructural observations of annealed samples suggest that an increase in porosity is manifested in trails of unconnected pores along grain boundaries. Particularly large pores are found surrounding wollastonite-rimmed quartz grains.

Pore pressure depends on pressure and temperature, on the fluid volume in the pores, and on fluid composition. At the onset of the decarbonation reaction the pores in the specimens contain air and argon. Since the starting material is almost impermeable, pore pressure is probably close to confining pressure. After start of the

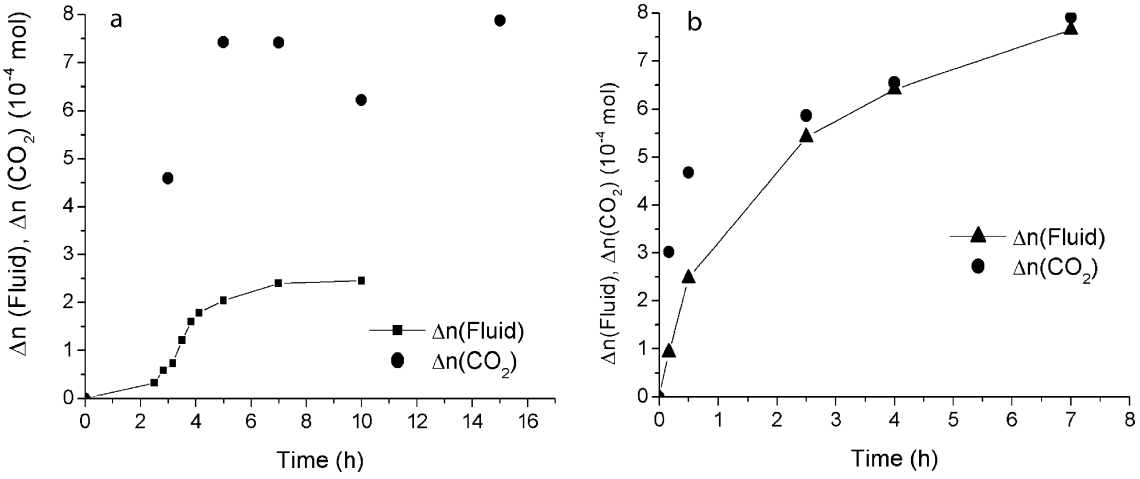

Fig. 7 Comparison of the molar amount of released fluid estimated from pore pressure increase Δn (fluid) and calculated from wollastonite rim thicknesses Δn (CO_2): **a** at 300 MPa confining pressure and 950 °C (run no. 78; run nos. 73, 76, 77, 78, 80); **b** at 150 MPa confining pressure and 950 °C (run no. 100; run nos. 95/96, 97, 98, 99, 100). Values are from Table 1

reaction, sample porosity increased by about a factor of two. Porosity increase was strongest at the onset of the reaction and then remained almost constant (Fig. 4). This was also observed by Ko et al. (1997) during gypsum dehydration. They suggested that the strong initial porosity increase slowed down the observed pore pressure increase in stage (1), because a large fraction of produced fluid was stored in the sample. This seems unlikely for the CO_2-forming reaction between calcite and quartz for which a positive excess volume is generated at 300 MPa pressure and 950 °C (Churakov and Gottschalk, 2003).

Since sample porosity is isolated at the onset of the reaction we can reasonably assume that the fluid pressure in the pore space is close to confining pressure. Before the reaction starts the pore fluid is mainly composed of air, CO_2, and argon. Once the reaction starts, the pore fluid becomes rapidly enriched in CO_2. Modeling pore pressures for binary mixtures of H_2O-CO_2 shows a dramatic increase in total pressure with increasing x_{CO2} even at a very small reaction turnover (Labotka et al. 2002). As ΔV of the wollastonite-producing reaction is positive, pore pressure will increase rapidly as soon as the reaction starts, particularly at low initial porosity. Therefore, pore stretching and the formation of cracks are most likely to occur immediately after the onset of the reaction. Variable delays of fluid pressure increase in the downstream reservoir during the initial stage (1) possibly reflect the time required to establish a connected crack network. The observed variable delays depend on sample composition, effective confining pressure and on microstructural variations between different samples.

In most experiments, maximum CO_2-release from the reaction between calcite and quartz occurs stepwise. This fluid expulsion process is very different from the one observed in experiments performed by Zhang et al. (2000) at lower temperatures of < 700 °C and in the presence of water at much higher initial porosities of 20%. At their experimental conditions, fluid release was continuous, and sample porosity and permeability were high. However, at temperatures > 700 °C, permeability dropped to $k < 1\times10^{-21}$ m^2 and measurements were no longer possible, in agreement with our observations.

Similarly, Ko et al. (1997) reported continuous release of H_2O from the reaction of gypsum to bassanite. They suggested that dehydration accelerated in stage (2) as pores coalesced and sample permeability was enhanced. However, at the conditions of their experiments with relatively low temperatures of ≤ 150 °C, compaction of the rock matrix during fluid release did not destroy a connected network.

In this study, monitoring of sample permeability during annealing and reaction suggests that a persistent fluid pathway did not exist across the entire length of the sample. Instead, formation of a transient crack network in the specimen occurred owing to buildup of pore pressure from the CO_2-producing reaction. The wollastonite-forming reaction and CO_2 expulsion are directly linked to significant microstructural changes (Fig. 3c–f). Pores decorating grain boundaries are ubiquitous in samples that showed step-wise pore pressure increase and fluid release. We interpret these fluid inclusion trails as healed microcracks that were temporarily open during annealing (Fig. 3e). Episodic pore pressure increase and microstructure evolution suggest that connectivity of the pore space is short-lived and transient at high temperatures, thus draining local fluid reservoirs inside the sample to the pore pressure system. The resulting cycle includes pore pressure build-up, formation of a local crack network, pore pressure release and crack closure.

Plastic stretching and decrepitation of pores

Porosities of the annealed samples measured after quenching typically exceed the porosity estimates

based on reaction progress and increase of pore space calculated from the width of wollastonite rims by up to about 4% (Milsch 2000; Fig. 7a, b). This is probably due to plastic stretching of the pores located at the calcite/wollastonite interfaces at elevated pore pressures. The width of the pores was determined from SEM micrographs (Fig. 3c, d). For simplicity, we assume a spherical geometry of the pore volume located at the phase boundaries resulting from solid volume reduction and pore stretching. The radial component of the strain rate of an expanding spherical pore $\dot{\varepsilon}_r$ may be expressed as:

$$\dot{\varepsilon}_r = d(\Delta r/r_0)/dt \tag{1}$$

where r_0 is a starting pore radius assuming reaction is completed and Δr is the measured pore radius minus r_0. For samples annealed at confining pressures of 300 and 150 MPa, $\dot{\varepsilon}_r$ is about 2×10^{-6} s^{-1} and 4×10^{-6} s^{-1}, respectively. Using the model for plastic deformation of isolated spherical pores from Wilkinson and Ashby (1975) and including grain size sensitivity, the radial strain rate component $\dot{\varepsilon}_r$ at a given distance r from the inclusion is:

$$\dot{\varepsilon}_r = \frac{2}{r^3} A d^{-m} \exp(-Q/RT) \frac{(r_0 b)^3}{(b^{3/n} - r_0^{3/n})^n} \left[\frac{3|P_c - P_f|}{2n}\right]^n \tag{2}$$

where A is a pre-exponential constant, d is grain size, m is the grain size exponent, Q is the creep activation energy, T is temperature, R is the universal gas constant, n is the stress exponent, and b is the distance to an elastically relaxed region (i.e. a grain boundary or crack).

Assuming $A = 10^{4.93}$ MPa s^{-1} μm$^{1.87}$, $Q = 190$ kJmol^{-1}, $n = 1.67$, $m = 1.87$ (Walker et al., 1990), $T = 1223$ K, $r_0 = 15$ μm, $r = 17$ μm and $b = 25$ μm, excess pore pressures $|P_c - P_f|$ of about 0.6 and 1 MPa, respectively, are required for pore stretching at radial strain rates $\dot{\varepsilon}_r$ of 2×10^{-6} s^{-1} and 4×10^{-6} s^{-1}.

This indicates that pore stretching will occur immediately once the pore pressure starts to exceed the confining pressure. We assume that the long-term excess pore pressure inside the specimens never exceeded about 20 MPa during the experiments (see below).

When the fluid pressure P_f developing in the pore space exceeds the confining pressure P_c reaching a critical value, pores will start to decrepitate and the pore fluid will be released. The critical pore pressure P_{crit} at which a spherical pore decrepitates is of the form:

$$P_{crit} = (P_f - P_c) = K_{1c} / \left[1.68(\pi a)^{1/2}\right] \tag{3}$$

(Lawn and Wilshaw 1975; Atkinson 1984; Wanamaker et al. 1990), where K_{Ic} is the critical stress intensity factor of the matrix and a denotes the half length of an initial crack emanating from the pore.

Neglecting the temperature dependence of fracture toughness, the critical pore pressure is estimated using available data at room temperature. For calcite, K_{Ic} ranges from 0.16–0.20 MPa m$^{1/2}$ (Gilman 1960; Santhanam and Gupta 1968; Atkinson and Avdis 1980). Using $K_{Ic} = 0.2$ MPa m$^{1/2}$ and assuming that the initial flaw size is of the order of the grain size, i.e. $a = 10$ μm, P_{crit} is about 20 MPa. This compares well with the uniaxial tensile strength of fine grained limestone of 10–20 MPa (Rummel 1982).

Crack healing

Presumably, the collapse of pore space and crack healing alternated with cyclic fluid drainage in our experiments. Release of CO_2 led to a drop in pore pressure and concomitant crack closure. Plots of pore pressure versus annealing time often show erratic steps, however, the time intervals between larger pressure steps typically exceeded 15–30 min. Crack healing rates in calcite increase rapidly with temperature and effective confining pressure, but depend inversely on crack apertures (Hickman and Evans 1987; Zhang et al. 2001), which are unknown for our samples. Healing rates are faster for intergranular cracks compared to grain boundary cracks (Olgaard and Fitzgerald 1993; Zhang et al. 2001). Zhang et al. (2001) and Hickman and Evans (1987) found crack tip regression rates up to about 1×10^{-2} μm.s^{-1} at temperatures between 550–850 °C. Since our samples were annealed at 900–1000 °C, it is likely that the crack network was partly destroyed disconnecting local CO_2 reservoirs at annealing times <60 minutes.

Implications for natural systems

Wollastonite is typically formed in marbles and metaargillites at the inner and hotter parts of contact metamorphic aureoles. Its occurrence and spatial distribution within a specific aureole, along with shifts in stable isotope geochemistry of coexisting minerals and host rocks, have been extensively used to document volatile producing mineral reactions controlled by fluid compositions (Baumgartner and Valley 2001; Ferry et al. 2002; and references therein). There are many examples for externally derived magmatic fluids introduced along metamorphic aquifers, which typically follow lithological boundaries (e.g. Heinrich 1993; Jamtveit et al. 1992). There are also many cases, often within the same aureoles, where rock units, particularly thick-bedded marbles, were essentially impermeable for external fluids (ref. above; Joesten and Fisher 1988). In the latter, fluid compositions were internally buffered and CO_2 was produced at water-absent conditions, similar to our experiments. In most field studies, however, the mechanism of CO_2 release remains unclear, even for the apparently simple internally buffered system.

Patterns of fluid flow based on mineralogical and stable isotope evidence are commonly predicted using the simplifying assumption of a continuous and constant porosity and permeability during decarbonation of the rock (Baumgartner and Valley 2001; Ferry et al. 2002; and references therein). Our experiments show that simple flow models, which assume constant pore pressure, constant fluid-filled porosity, and constant permeability are not appropriate (see also Buick and Cartwright 2002). These properties are rather transient and it is most likely that fluid flow in a specific reacting rock volume is a very short-lived process.

The occurrence of vein-filled and open cracks in deformed rocks is often related to the presence of elevated pore pressures that are likely to exist where metamorphic fluids are released. Hydro-fracturing possibly assists in focused flow of such metamorphic fluids through a low-permeability host rock (Walther and Orville 1982; Thompson 1997), but the importance of hydro-fracturing for drainage of metamorphic fluids on a crustal scale is still a matter of debate (Connolly 1997). In agreement with theoretical models (Labotka et al. 2002) our experiments suggest that reaction-induced pore pressures quickly reach the critical value required for hydro-fracturing, provided that host rock permeability is low and generated fluids cannot be released rapidly enough.

Conclusions

The investigation of the effect of the wollastonite-forming decarbonation reaction calcite + quartz = wollastonite + CO_2 on the transport properties of rocks performed in this study at a confining pressure of up to 300 MPa, temperatures up to 950 °C and at water-absent conditions leads to the following conclusions:

Compaction of the ductile matrix results in a low-porosity and low-permeability rock matrix. Pore pressure in unconnected porosity equilibrates with confining pressure and the effective pressure acting on the rock sample is close to zero.

Fluid expulsion from the almost impermeable matrix occurs predominantly episodic. Pore pressure pulses depend on boundary conditions, composition and starting microstructure of the material.

As bulk sample permeability remained low during annealing and reaction, we suggest that fluid transport occurred as a local process on the grain scale.

Acknowledgements Harald Milsch acknowledges the financial support from the GeoForschungsZentrum whilst performing his Ph.D. Michael Naumann kept the gas medium apparatus running and Erik Rybacki is thanked for many constructive suggestions and discussions. SEM-microscopy was supported by Ursula Glenz. Harald Milsch appreciates his internship at MIT with Brian Evans and Gunter Siddiqi, which was co-financed by a NATO stipend. Thoughtful comments by R. Abart and B. Jamtveit are gratefully acknowledged.

References

Atkinson BK (1984) Subcritical crack growth in geological materials. J Geophys Res 89:4077–4114

Atkinson BK, Avdis V (1980) Fracture mechanics parameters of some rock-forming minerals determined using an indentation technique. Int J Rock Mech Min Sci Geomech Abstr 17:383–386

Baud P, Zhu W, Wong TF (2000) Failure mode and weakening effect of water on sandstone, J Geophys Res 105:16371–16389

Baumgartner LP, Valley JW (2001) Stable isotope transport and contact metamorphic fluid flow. In:Valley JW, Cole DR (eds) Stable isotope geochemistry (Reviews in Mineralogy and Geochemistry, vol 43) Mineral Soc Am, Washington, DC, pp 415–467

Bernabé Y, Brace WF, Evans B (1982) Permeability, porosity and pore geometry of hot-pressed calcite. Mech Mater 1:173–183

Brace WF, Paulding BW, Scholz C (1966) Dilatancy in the fracture of crystalline rocks. J Geophys Res 71:3939–3953

Buick IS, Cartwright I (2002) Fractured-controlled fluid flow and metasomatism in the contact aureole of the Marulan Batholith (New South Wales, Australia). Contrib Mineral Petrol 143:733–749

Churakov SV, Gottschalk, M (2003) Perturbation theory based equation of state for polar molecular fluids: II. Fluid mixtures. Geochim Cosmochim Acta 67:2415–2425

Connolly JAD (1997) Devolatilization-generated fluid pressure and deformation propagated fluid flow during prograde regional metamorphism. J Geophys Res 102:18149–18173

Connolly JAD, Holness MB, Rubie DC, Rushmer T (1997) Reaction-induced microcracking: an experimental investigation of a mechanism for enhancing anatectic melt extraction. Geology 25:591–594

Etheridge MA, Wall VJ, Vernon RH (1983) The role of the fluid phase during regional metamorphism and deformation. J Metamorph Geol 1:205–226

Etheridge MA, Wall VJ, Cox SF, Vernon RH (1984) High fluid pressures during regional metamorphism and deformation: Implications for mass transport and deformation mechanisms. J Geophys Res 89:4344–4358

Feenstra A, Wunder B (2002) Dehydration of diasporite to corundite in nature and experiment. Geology, 30:119–122

Ferry JM (1994) A historical review of metamorphic fluid flow. J Geophys Res 99:15487–15498

Ferry JM, Wing BA, Penniston-Dorland SC, Rumble DIII (2002) The direction of fluid flow during contact metamorphism of siliceous carbonate rocks: new data for the Monzoni and Predazzo aureoles, northern Italy, and a global review. Contrib Mineral Petrol 142:679–699

Fischer GJ (1992) The determination of permeability and storage capacity: Pore pressure oscillation method. In: Evans B, Wong TF (eds) Fault mechanics and transport properties of rocks. Academic Press, San Diego, pp 187–211

Fischer GJ, Paterson MS (1992) Measurement of permeability and storage capacity in rocks during deformation at high temperature and pressure. In: Evans B, Wong TF (eds) Fault mechanics and transport properties of rocks. Academic Press, San Diego, pp 213–252

Gilman JJ (1960) Direct measurements of the surface energies of crystals. J Appl Phys 31:2708–2718.

Gottschalk M (1997) Internally consistent thermodynamic data set for rock forming minerals in the system SiO_2-TiO_2-Al_2O_3-Fe_2O_3-CaO-MgO-FeO-K_2O-Na_2O-H_2O-CO_2: an alternative approach. Eur J Mineral 9: 175–223

Harker RI, Tuttle OF (1956) Experimental data on the P_{CO2}–T curve for the reaction: calcite + quartz↔wollastonite + carbon dioxide. Am J Sci 254:239–256

Heinrich W (1993) Fluid infiltration through metachert layers at the contact aureole of the Bufa del Diente intrusion, northeast Mexico: Evidence from stable isotopes. Contrib Mineral Petrol 119:362–376.

Heinrich W, Hoffbauer R, Hubberten HW (1995): Contrasting fluid flow patterns at the Bufa del Diente contact metamorphic aureole, north-east Mexico: evidence from stable isotopes. Contrib Mineral Petrol 119:362–376

Hickman SH, Evans B (1987) Influence of geometry upon crack healing rate in calcite. Phys Chem Miner 15:91–102

Jamtveit B, Bucher-Nurminen K, Stijfhoorn DE (1992) Contact metamorphism of layered shale-carbonate sequences in the Oslo rift. I. Buffering, infiltration, and the mechanisms of mass transport. J Petrol 33:377–422

Joesten R, Fisher G (1988) Kinetics of diffusion-controled mineral growth in the Christmas Mountains (Texas) contact aureole. Geol Soc Am Bull 100:714–732

Kirby SH, Engdahl ER, Denlinger R (1996) Intermediate-depth earthquakes and arc volcanism as physical expressions of crustal and uppermost mantle metamorphism in subducting slabs. In: Bebout GE, Scholl DW, Kirby SH, Platt JP (eds) Subduction, top to bottom. Geophys Monogr 96, pp 195–214

Ko Sc, Olgaard DL, Briegel U (1995) The transition from weakening to strengthening in dehydrating gypsum: Evolution of excess pore pressures. Geophys Res Lett 22:1009–1012

Ko Sc, Olgaard DL, Wong TF (1997) Generation and maintenance of pore pressure excess in a dehydrating system. 1. Experimental and microstructural observations. J Geophys Res 102:825–839

Labotka TC, Anovitz LM, Blencoe JG (2002) Pore pressure during metamorphism of carbonate rock: effect of volumetric properties of H_2O-CO_2 mixtures. Contrib Mineral Petrol 144:305–313

Lawn BR, Wilshaw TR (1975) Fracture of brittle solids. Cambridge University Press, New York, 204 pp

Miller SA, Nur A (2000) Permeability as a toggle switch in fluid-controlled crustal processes. Earth Planet Sci Lett 183:133–146

Milke R, Heinrich W (2002) Diffusion-controlled growth of wollastonite rims between quartz and calcite: comparison between nature and experiment. J. Metamorph Geol 20:467–480

Milsch H (2000) Experimentelle Untersuchung des Einflusses von Dekarbonatisierungs-reaktionen auf die Transporteigenschaften von Gesteinen. PhD Thesis, Faculty of Natural Sciences, University of Potsdam, Germany, 126 pp

Olgaard DL, FitzGerald JD (1993) Evolution of pore microstructures during healing of grain boundaries in synthetic calcite rocks. Contrib Mineral Petrol 115:138–154

Olgaard DL, Ko Sc, Wong TF (1995) Deformation and pore pressure in dehydrating gypsum under transiently drained conditions. Tectonophysics 245:237–248

Raleigh CB, Paterson MS (1965) Experimental deformation of serpentinite and its tectonic implications. J Geophys Res 70:3965–3985

Rummel F (1982) Fracture and flow of rocks and minerals. In: Landolt-Börnstein Group V: Geophysics 1B. Springer, Berlin Heidelberg New York, pp 141–239

Rutter EH, Brodie KH (1988) Experimental syntectonic dehydration of serpentinite under conditions of controlled pore water pressure. J Geophys Res 93:4907–4932

Rumble DIII, Ferry JM, Hoering TC, Boucot AJ (1982). Fluid flow during metamorphism at the Beaver Brook fossil locality, New Hampshire. Am J Sci 282:886–919

Santhanam AT, Gupta YP (1968) Cleavage surface energy of calcite. Int J Rock Mech Min Sci 5:253–259

Scholz CH, Sykes LR, Aggarwal YP (1973) Earthquake prediction: a physical basis. Science 181:803–810

Simpson G, Gueguen Y, Schneider F (2001) Permeability enhancement due to microcrack dilatancy in the damage regime. J Geophys Res 106:3999–4016

Tanner SB, Kerrick DM, Lasaga AC (1985) Experimental kinetic study of the reaction: calcite + quarz↔wollastonite + carbon dioxide, from 1 to 3 kilobars and 500 to 850 °C. Am J Sci 285:577–620

Thompson AB (1997) Flow and focusing of metamorphic fluids. In: Jamtveit B, Yardley B (eds) Fluid flow and transport in rocks. Chapman and Hall, New York, pp 297–314

Urai JL, Feenstra A (2001): Weakening associated with the diaspore-corundum dehydration reaction in metabauxites: an example from Naxos (Greece). J Struct Geol 23:941–950

Walker AE, Rutter EH, Brodie K (1990) Experimental study of grain-size sensitive flow of synthetic, hot-pressed calcite rocks. In: Knipe RJ, Rutter EH (eds) Deformation, mechanisms, rheology and tectonics. Geol Soc Spec Publ, London, pp 259–284

Walther JV, Orville PM (1982) Volatile production and transport in regional metamorphism, Contrib Mineral Petrol 79:252–257

Wanamaker BJ, Evans B (1989) Experimental diffusional crack healing in olivine. In: Schock RN (ed) Point defects in minerals. Am Geophys Union, Geophys Monograph 31, pp 194–210

Wanamaker BJ, Wong TF, Evans B (1990) Decrepitation and crack healing of fluid inclusions in San Carlos olivine. J Geophys Res 95:15623–15641

White SH, Knipe RJ (1978) Transformation- and reaction-enhanced ductility in rocks. J Geol Soc Lond 135:513–516

Wilkinson DS, Ashby MF (1973) Pressure sintering by power-law creep. Acta Metall 23:1277–1285.

Wong TF, Ko Sc, Olgaard DL (1997) Generation and maintenance of pore pressure excess in a dehydrating system. 2. Theoretical analysis. J Geophys Res 102:841–852

Zhang S, Paterson MS, Cox SF (1994) Porosity and permeability evolution during hot isostatic pressing of calcite aggregates. J Geophys Res 99:15741–15760

Zhang S, FitzGerald JD, Cox SF (2000) Reaction-induced permeability during decarbonation of calcite + quartz → wollastonite + carbon dioxide. Geology 28:911–914

Zhang S, Paterson MS, Cox SF (2001) Microcrack growth and healing in deformed calcite aggregates. Tectonophysics 335:17–36